QUALITY FACTORS OF MEMS GYROS AND THE ROLE OF THERMOELASTIC DAMPING

Amy Duwel, Marcie Weinstein, John Gorman, Jeff Borenstein, Paul Ward
The Draper Laboratories, Cambridge, MA
Massachusetts Institute of Technology, Cambridge, MA

Abstract – **In this paper, we present new experimental data illustrating the importance of thermoelastic damping in MEMS resonant sensors. We have used MEMS gyroscopes to demonstrate that both the choice of materials and variations in device design can lead to significant differences in the measured Quality (Q) factors of the device. These differences in Q factor can be explained by including the contribution of thermoelastic damping (TED), which varies strongly between the different silicon etch-stop compositions used in this study. Known damping mechanisms such as fluid damping, anchor damping, and electronics damping are minimized and held fixed in this experiment so that materials effects can be isolated.**

I. INTRODUCTION

Thermoelastic damping has been identified as an important loss mechanism in MEMS resonators [1-3]. The impact of device geometry on the level of damping has been considered both experimentally and theoretically [3-5]. Although most work to date has focused on analytically tractable beam systems, the need for high Q resonators extends to a wide variety of applications, including accelerometers [6], Coriolis rate sensors [7], chemical sensors [8], and RF filters [9]. In most applications, maintaining a high Quality factor results in reduced readout errors, lower power requirements, improved stability, and increased sensitivity.

The resonator devices used in this study were MEMS gyros fabricated at Draper Laboratory. The excitation and readout mechanism is capacitive, and the measurements are made in a vacuum better than 1 mTorr. We find that the simple calculation by Zener [1-2] for thermoelastic damping in flexural mode beam resonators works well to describe the effects of beam width and material properties on the Q factor of the resonant-mode gyros. In this paper, the effects of alloying on thermal conductivity and the resulting effect on Q factor are explored. We compare measurements on devices made from silicon-germanium alloys with Ge concentrations of up to 30%, and with boron doping of up to $2x10^{20}$ cm^{-3}. Using thermal conductivity data from Dismukes [10] on Boron doped SiGe materials, we show that the differences in thermal conductivity can account for our observed Q factors.

In Section II, we introduce the MEMS resonator being studied and the experimental setup. We also discuss the impact of our measurement setup on the measured Q of the resonator. In Section III we review thermoelastic damping and discuss some of the important material parameters that must be known to quantify this effect. Section IV compares a theory for total Q-factor to measured data.

II. EXPERIMENTAL SETUP

The MEMS gyro is a tuning fork resonator which senses angular rate. A photograph of the gyro (top view) is shown in Figure 1. The masses are driven in a tuning fork resonance mode in the plane of the wafer. In response to an angular rate, the two proof masses move out of the wafer plane ($\pm \hat{y}$) in opposite directions. This motion is sensed capacitively and the amplitude of this motion is the desired signal, proportional to angular rate.

In the design of resonant sensors, the readout circuit must balance the need for low insertion loss with high Q factor. Any output signal current, for example, results from a coupling to the resonating sensor and can lead to dissipation of the mechanical resonance [11]. Draper's gyros use a capacitive readout where the resonator mass serves as one plate of a capacitor. The other "plate" is fixed to the substrate. The motion of the resonator causes a changing capacitance. In the presence of a voltage bias, a current is read out from either the proof mass itself or from the fixed plate. The current is defined by $I = \dot{C}V + \dot{V}C$, and for the case of a DC bias is simply proportional to the

0-7803-7185-2/02/$10.00 ©2002 IEEE

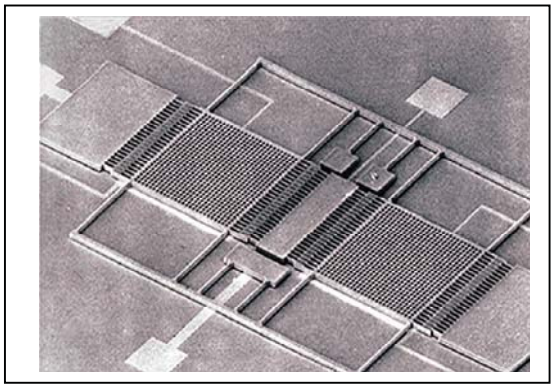

Figure 1: Photograph of a Draper tuning fork gyro.

proof mass motion through $\dot{C} = \dot{u}\, dC/du$, where u is the amplitude of motion in the x-direction. This current is amplified and converted to a voltage, and the transfer function of the output to the input voltage is used to measure Q. Figure 2 shows the circuit schematic used to drive the sensor and measure the Q value. For Q measurements, the input drive voltage is the sum: $V_{drive} = V_{DC} + V_{in} \sin \omega t$, so that the force on the sensor is:

$F_{drive} = V_{DC}^2 + V_{DC} V_{in} \sin \omega t + V_{in}^2 \sin^2 \omega t$. The transfer function is taken by comparing V_{out} at ω to V_{in}.

We use the half power bandwidth relative to the resonant frequency to measure the Q. This works well as long as drive coupling to other modes is minimized and the spectrum looks like that of an isolated resonator. When using this method, it is also important to drive the resonator at low amplitudes, so that nonlinear effects are negligible. Bandwidth and ringdown testing[1] typically agreed to better than 10 % even without taking the different bias conditions and corresponding electrostatic spring effects into account. The resonance peaks were very symmetric, and the standard deviation of the repeated bandwidth measurements is 1%. All measurements were conducted at the wafer level under a vacuum of approximately 1mTorr.

[1] Note that both bandwidth and ringdown tests for measuring Q will be affected by the presence of nearby modes. According to theory [Nayfeh], ringdown tests should not be affected by amplitude nonlinearities. For small drive amplitudes, the effects of amplitude nonlinearities on resonance curve measurements can also be minimized.

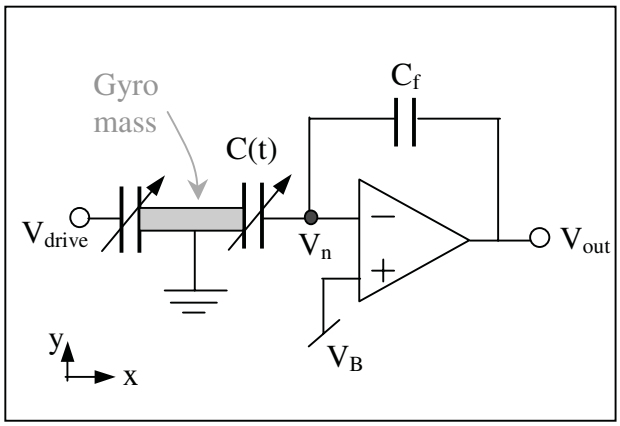

Figure 2: Circuit schematic of capacitive readout for MEMS resonator. The mode of interest results in a movement of the gyro mass in the x-z plane. The gyro resonance is excited on one side of the mass by an electrostatic force and the change in the readout capacitance is sensed. Comb finger capacitors are used so that the readout is linear in x.

The measurement itself can influence the Quality factor of the gyro. In order to produce a signal out, power has to be coupled from the resonator, and this power can be dissipated. We include in the appendix a simple model for the gyro dynamics and the role of the applied voltages. We use this model to calculate the electronics contribution to the Q factor and include it in the total calculated Q. Since all of our gyro designs use almost identical input and output coupling capacitors, the contribution of the electronics damping does not vary from device to device.

III. THERMOELASTIC DAMPING

Thermoelastic damping arises from the coupling of the stress-strain state equation to heat flow in the material. The familiar effects of the coefficient of thermal expansion (α), where stresses (σ) and strains (ε) can be thermally induced, can be derived from the dependence of the Hemholtz Free Energy on both strain and temperature. From this starting point, however, one also finds that the temperature gradient in a material can be driven by changes in strain. The coupled (linearized) state equations for an isotropic medium are [12,13]:

Table 1: Material and device parameters used in thermoelastic damping calculations. The notation "Int" refers to a linear interpolation between the silicon and germanium values, based on the alloy composition.

Quantity	Symbol	Units	SiB epi	SiGeB 2%	SiGeB 23%	SiGeB 30%	B-diff	Si Value	Ge Value
Thermal Coefficient of Expansion	α	1/°C	2.57E-06	2.65E-06	3.33E-06	3.55E-06	2.59E-06	2.59E-06	5.80E-06
reference			Si value	Int	Int	Int	[21]	[17],[18]	[18]
Modulus	E	N /m^2	1.69E+11	1.68E+11	1.54E+11	1.49E+11	1.69E+11	1.69E+11	1.03E+11
reference			Si value	Int	Int	Int	Si value	[18]	[18]
Density	ρ	kg/m^3	2.33E+03	2.39E+03	3.02E+03	3.24E+03	2.33E+03	2.33E+03	5.35E+03
reference			Si value	Int	Int	Int	Si value	[17]	[18]
Specific Heat	$C_{sp}=C_V/\rho$	J/(K*kg)	7.00E+02	7.05E+02	6.23E+02	5.95E+02	7.00E+02	7.13E+02	3.20E+02
reference			Si value	Int	Int	Int	Si value	[20]	
Thermal Conductivity	K	J/(K*s*m)	80	10.67	5.71	5.52	80.00	1.56E+02	58.61
reference			[22,16]	[22,16]	[22,16]	[22,16]	[22,16]	[18],[20]	[18]
Time Constant	τ	s	9.00E-08	7.62E-07	1.40E-06	1.54E-06	7.44E-08		
Beam Width	b	m	6.60E-06	6.90E-06	6.48E-06	6.60E-06	6.00E-06		
Resonant Frequency	$f=\omega/2\pi$	Hz	12,851	13,327	10,357	10,785	12,361		
Thermoelastic Q value	Q_{TED}		6.70E+05	7.48E+04	4.07E+04	3.30E+04	8.29E+05		

(1) $$\varepsilon = \frac{\sigma}{E} + \alpha T$$

(2) $$\frac{dT}{dt} = \frac{\kappa}{C_V}\nabla^2 T - \frac{E}{1-2\nu}\frac{\alpha T_o}{C_V}\frac{d\varepsilon}{dt}$$

where E is the Young's modulus, ν is Poisson's ratio, T_o is the nominal equilibrium temperature, and T is the temperature offset from equilibrium. The coefficient of thermal expansion is α, the thermal conductivity is κ, and the heat capacity at constant volume is C_v.

An effective transfer function for stress versus strain can be found by assuming linear solutions and eliminating temperature [4,14]. However, the linear solutions to the heat equation depend on the boundary conditions, and in small-scale devices these can play an important role. The derived transfer function can be treated as an effective Young's modulus and becomes part of the spring constant for a given resonator. In the transfer function derived from combining the equations above, the combination of a zero followed closely by a pole results in a resonance in the imaginary component of the modulus called a Debye peak. The resonance frequency appears at the characteristic time for heat flow in the system, which depends on both the thermal conductivity of the material as well as the boundary conditions. The Quality factor derived by Zener [1-2] for a flexural mode beam resonator becomes:

(3) $$Q_{TED}^{-1} = \frac{E\alpha^2 T_o}{C_V}\frac{\omega\tau}{1+(\omega\tau)^2}$$

with

(4) $$\tau = \frac{C_V b^2}{\kappa\pi^2}$$

where ω is the mechanical resonance frequency of the beam and b represents the width of the resonator in the plane of the resonance motion.

In the resonators tested, several different materials were tested. We especially focused on Boron-doped SiGe epitaxial materials since the presence of Ge reduces strain in the epi layer and the resulting devices can be extremely flat and well-machined. In addition, the use of Ge as an etch stop eliminates the need for EDP in processing [15], which is a huge advantage. However, considering the issue of thermoelastic damping, the use of an alloy can significantly reduce the thermal

conductivity due to phonon scattering. Based on the data of Dismukes [10], we summarize in Table 1 the material parameters used for the calculation of Q_{TED}. We also measured devices made from Boron diffused silicon (noted as B-diff in the plots), where the Boron concentration was approximately 10^{21}. Although the Debye resonance frequency ($1/\tau$ in Table 1) is orders of magnitude above our operating frequency of about 12 kHz, the importance of the thermal conductivity is apparent when we compare the theory to our measurements.

IV. DATA VERSUS THEORY

The total damping in the resonators can be calculated from combining the known mechanisms:

$$\frac{1}{Q_{tot}} = \frac{1}{Q_{electronics}} + \frac{1}{Q_{TED}} + \frac{1}{Q_{other}} \quad (5)$$

In the calculated Q_{tot}, we use Q_{other} as a fitting parameter for our data. This Q_{other} represents as yet un-modeled effects such as anchor damping, any residual gas damping, and other material losses. If it turns out that the differences in Q_{TED} between materials tested can explain our data, then a single value of Q_{other} will fit all of the data well. In fact, we find that for a single device design, Q_{other} = *250,000* works well for all the materials measured. The plot in Figure 3 compares the data to the theory. The electronics damping was in the range of $Q_{electronics} = 3.5*10^{11}$ but varies slightly between devices since the undercut (which we measure to be typically less than 0.5 μm) can affect the readout capacitor size. The thermoelastic Q values are listed in Table 1.

In addition to the data presented in Figure 3, we also compared the measured Q values of various device designs. In several iterations of the tuning fork gyro, the beam widths were varied to optimize the modes of the devices. Based only on the beam width and resonance frequency data, we have been able to use thermoelastic damping to explain why some designs exhibited much higher Q values than others. The match of thermoelastic damping theory to our data over a range of device designs indicates that the anchor damping does not vary much between these iterations. However, the relatively low best fit values of Q_{other} = *250,000* suggest that anchor damping may be an important limiting factor.

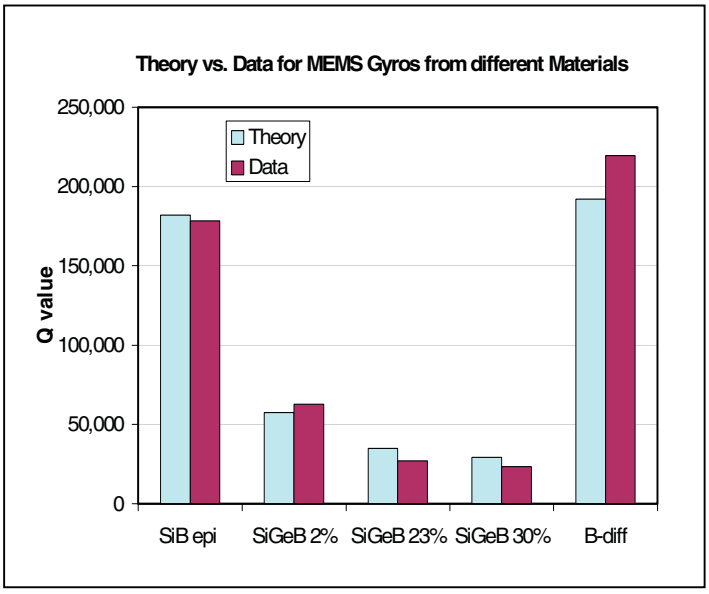

Figure 3: Data versus calculated Q values. In the theory, Q_{other} = 250,000 is used as a fitting parameter.

V. CONCLUSIONS

We have measured the Quality factors of resonators made from several different semiconductor materials. Our data can be explained well by thermoelastic damping and electronics damping calculations. Despite the fact that thermoelastic damping is not the limiting factor in our devices, changes in Q_{TED} can affect our final measured Q values by factors of two and three. Understanding the importance of this mechanism has led to improved designs, where both material properties and geometry are optimized to achieve the highest Q possible. Future work in modeling and minimizing the additional loss mechanisms such as anchor damping will further improve MEMS resonator designs.

APPENDIX: CALCULATION OF ELECTRONICS DAMPING

The tuning fork resonance is excited by applying an AC voltage to the outer capacitor (left capacitor in Figure 2). The electrostatic force on the gyro is proportional to the square of the drive voltage. At the output, the voltage bias needed to generate a readout signal can also place a force on the sensor. To model the system dynamics, we balance these electrostatic forces on the sensor with the inertia and resorting force on the masses. The

force balance becomes simplest when the motion of the resonator is already decomposed into linear eigenmodes. For the tuning fork mode of interest, the masses move in the wafer plane, in the x-direction of Figure 2. The modal amplitude is represented by *u(t)*, and the force balance becomes:

$$(6)\quad m\ddot{u} + b\dot{u} + ku = \frac{(V_{drive})^2}{2}\frac{dC}{du} + \frac{(V_n)^2}{2}\frac{dC}{du}$$

The electrostatic forces in (6) are proportional to the change in capacitance with sensor mode amplitude. For these gyros, the drive and sense capacitors on the motor axis are comb designs, and to first order the term *dC/du* is a constant that depends on geometry but is independent of *u*. In equation (6), *m* is the modal mass and *b* is the modal damping from sources other than the electronics.

If the amplifier gain is infinite, the node voltage V_n is equal to V_B. The gain is assumed to be purely imaginary at the operating frequency. For finite gain, we write:

$$(7)\quad V_n = V_B - I_s R_{in}$$

$$(8)\quad I_s = \dot{C} V_n$$

$$(9)\quad R_{in} = \frac{1}{\omega C_f |A|}$$

I_s is the sensor current, R_{in} is the input resistance of the op-amp, and A is the amplifier gain. These equations combine to give:

$$(10)\quad V_n = \frac{V_B}{1 + \dot{u}(dC/du)R_{in}}$$

For large amplifier gain, R_{in} is small and a Taylor expansion can be applied to (10). In the limit of large amplifier gain, equation (6) becomes:

$$(11)\quad m\ddot{u} + b\dot{u} + ku = \frac{(V_{drive})^2}{2}\frac{dC}{du} + \frac{(V_B)^2}{2}\frac{dC}{du} - (V_B)^2\frac{dC}{du}R_{in}\dot{u}$$

Thus the applied bias results in a term proportional to velocity. By taking the ratio of stored energy to the energy dissipated per cycle, the contribution of the electronics to the Q of the system is:

$$(12)\quad Q_{electronics} = \frac{mC_f|A|\omega^2}{2V_B^2(dC/du)^2}$$

Note that designing for large readout gains (high V_B and *dC/du*) can degrade the resonator Q value. However, the readout amplifier gain can compensate for this effect.

ACKNOWLEDGEMENT

The authors wish to thank Robert White for his initial measurements of Q factors in gyros and Bill Sawyer for assistance with the fabrication. We especially thank Mark Mescher for valuable conversations. We also thank Marc Weinberg, Chris Dubé and Richard Elliott for valuable advice and support.

REFERENCES

[1] C. Zener, *Physical Review* 52, Aug. 1, 1937; p 230.
[2] C. Zener, *Physical Review* 53, Jan. 1, 1938; p 90.
[3] T. V. Roszhart, *Proceedings of the Solid-State Sensor and Actuator Workshop, Hilton Head Island, SC*, 1990 (IEEE, New York, 1990), p. 13.
[4] R. Lifshitz, M. Roukes, *Phys. Rev. B*, vol 61 no 8, p. 61 (2000).
[5] K. Yasumura, T. Stowe, E. Chow, T. Pfafman, T. Kenny, B. Stipe, D. Rugar, *Journal of Microelectromechanical Systems*, vol 9 no 1, p. 117 (2000).
[6] Gibbons, Kevin A.; Borenstein, Jeffrey T.; Nokes, David S.; Weinberg, Mark S. "The design, fabrication, and testing of a micromechanical silicon oscillating accelerometer," *AIAA Guidance, Navigation, and Control Conference and Exhibit*, Boston, MA, Aug. 10-12, 1998, Collection of Technical Papers. Pt. 2 (A98-37001 10-63), pp. 1296-1306. 1998
[7] A. Kourepenis, J.T. Borenstein, J. Connelly, R. Elliott, P. Ward and M.S. Weinberg, "Performance of MEMS inertial sensors," *Conference: IEEE 1998 Position Location and Navigation Symposium*, 1 (1998).
[8] Weinberg, M.S.; Cunningham, B.T.; Clapp, C.W. "Modeling flexural plate wave devices," *Journal of Microelectromechanical Systems* , vol.9, no.3 , p. 370-9 Publisher: IEEE , Sept. 2000

[9] Kun Wang, Yinglei Yu, Ark-Chew Wong, and Clark T-C Nguyen, “VHF Free-Free Beam High-Q Micromechanical Resonators,” *Technical Digest*, 12th International IEEEE Micro Electro Mechanical Systems Conference, pp. 453-458 (1999).
[10] J. Dismukes, L. Ekstrom, E. Steigmeier, I. Kudman, D. Beers, *J. of Appl. Phys.,* vol 35 (10), Oct 1964.
[11] Varghese, Amantea, Sauer, Senturia, “Resistive Damping of Pulse-Sensed Capacitive Position Sensors,” *IEEE Transducers ’97*, p. 1121 (1997).
[12] Landau, Lifshitz, Theory of Elasticity. Pergamon Press, Oxford, 1959.
[13] Nowacki, Thermoelasticity, 2nd Edition, Chapter 1. Pergamon Press Ltd, 1986.
[14] R. Lakes, Viscoelastic Solids, p. 294-297. CRC Press LLC, 1999.
[15] Borenstein, J.T.; Gerrish, N.D.; Currie, M.T.; Fitzgerald, E.A. “A new ultra-hard etch-stop layer for high precision micromachining,” *Conference: Proceedings of 12th International Workshop on Micro Electro Mechanical Systems - MEMS , Sponsor: IEEE Robotics & Autom. Soc*, p. 205-10 (1999).
[16] K.L. Wang, X. Zheng, "Thermal properties of SiGe," in Properties of Strained and Relaxed Silicon Germanium, ed Erich Kasper, INSPEC, 1995.
[17] Y. Okada, "Diamond Cubic Si: structure, lattice parameter and density," in The Properties of Crystalline Silicon, ed. Robert Hull, INSPEC, 1999.
[18] http://www.webelements.com
[19] S.P. Baker, E. Arzt, "Elastic stiffness constants of SiGe," in The Properties of Silicon Germanium and SiGe:Carbon, ed Erich Kasper and Klara Lyutovich, INSPEC, 2000.
[20] H.-M. Kagaya, T. Soma, "Specific Heats of c-Si and molten Si," in The Properties of Crystalline Silicon, ed. Robert Hull, INSPEC, 1999.
[21] C. Cabuz, K. Fukatsu, T. Kurabayashi, K. Minami, M. Esashi, "Microphysical Investigations on Mechanical Structures Realized in p+ Silicon," *Journal of Microelectromechanical Systems*, vol 4 (3), Sept 1995.
[22] J. Dismukes, L. Ekstrom, E. Steigmeier, I. Kudman, D. Beers, "Thermal and Electrical Properties of Heavily Doped Ge-Si Alloys up to 1300K," *Journal of Applied Physics*, vol 35 (10), Oct 1964.